Nov 6th, 12:00 AM - 12:00 AM

Local Buckling Hysteretic Nonlinear Models for Cold-Formed Steel Axial Members

D. A. Padilla-Llano

C. D. Moen

M. R. Eatherton

Twenty-Second International Specialty Conference on Cold-Formed Steel Structures
St. Louis, Missouri, USA, November 5 & 6, 2014

Local Buckling Hysteretic Nonlinear Models for Cold-Formed Steel Axial Members

D.A. Padilla-Llano[1], C.D. Moen[2], M.R. Eatherton[3]

Abstract

This paper studies the energy dissipation and damage in thin walled members that experience local buckling and presents an approach to model cold-formed steel (CFS) axial members that experience local buckling deformations. The model is implemented in OpenSees using hysteretic models for CFS axial members calibrated using experimental responses. Results from thin-shell element simulations using ABAQUS show that energy dissipation in thin plates dissipates through inelastic strains and yielding that concentrates in damaged zones that extent approximately the length of a buckled half-wave (L_{cr}). Generally damage accumulates in one zone but when more than one damaged zone occurred the energy dissipation increased proportionally. The results from the plate simulation and experimental results from cyclic tests on axially loaded CFS members (previously performed by the authors) support the assumptions for the modeling approach presented for CFS members governed by local buckling. Results demonstrate the capabilities of the modeling approach to efficiently and accurately simulate the response of the CFS axial members experiencing local buckling. The model presented can be used to facilitate the performance assessment of cold-formed steel lateral load resisting systems (e.g., shear walls) under different hazard/performance levels, a capability needed for the advance of performance-based earthquake engineering of cold-formed steel buildings.

Introduction

The steel industry has increasing interest in using cold-formed steel (CFS) for multi-story building construction able to withstand earthquake induced lateral loads. These designs require the development of analysis tools and guidelines that allow safe design of actual CFS buildings. The research described herein supports

[1] Graduate Research Assistant, Virginia Tech, dapadill@vt.edu
[2] Associate Professor, Virginia Tech, cmoen@vt.edu
[3] Assistant Professor, Virginia Tech, meather@vt.edu

this seismic framework development with new insight on energy dissipation from local buckling.

Current analysis and prescriptive design procedures for CFS lateral load-resisting systems (e.g., steel/wood sheathed CFS shear walls), provide adequate protection against collapse (AISI 2007a), but lack the ability to predict and consider design performance levels. Such procedures cannot provide information about system and component energy dissipation, strength degradation, and stiffness degradation (e.g., drag struts and boundary chord studs). They also neglect the resistance from other CFS components that are not part of the lateral-load resisting system (e.g., gravity load supporting walls).

To develop proper seismic performance factors (i.e., R, Ω_0, and C_d) and include different hazard levels in addition to collapse, it is necessary to consider ground motions suites, many ground motion intensities, as well as, different structural layouts (FEMA 2009). This in turn translates into a sizable number of analyses (i.e., thousands of nonlinear response history analyses) that require accurate and computationally efficient models to simulate cyclic responses not only of the CFS lateral resisting systems but also their components and connections.

This paper presents a computationally efficient approach to model the cyclic response of cold-formed steel axial members that experience local buckling deformations. Energy dissipation in thin plates subjected to in-plane axial loading is studied to answers questions regarding how energy dissipates and where damage accumulates in members that experience local buckling deformations. The model parameters are derived based on the hysteretic energy dissipated and calibrated using cyclic responses from an experimental program conducted by Padilla-Llano et al. (2014), and implemented in OpenSees (Mazzoni et al. 2019).

Local buckling hysteretic nonlinear models for CFS axial members

Hysteretic models to accurately simulate CFS member axial cyclic responses should capture strength degradation, stiffness degradation, and pinching observed in typical responses such as the one shown in Figure 1a. Strength and stiffness degradation during cycling loading occurs due to buckling deformations in compression and yielding followed by tearing in tension (Padilla-Llano et al. 2014). Strength degradation is illustrated by the difference between the monotonic curve and the cyclic response envelope (Figure 1a). Stiffness degradation is illustrated by the difference in stiffness upon unloading after buckling occurs compared to the member initial stiffness k_o, (Figure 1a). Pinching occurs when buckling deformations straighten out during unloading and subsequent loading in

the opposite direction. In the tests conducted by Padilla-Llano et al. (2014), local buckling (i.e., web buckling) with multiple half-waves occurred before the peak compression load (Figure 2a). After the peak compression, one half-wave locked around mid-height and damage accumulated at that location as shown in Figure 2. Energy dissipation occurs due to post-peak cold-bending (in compression) and tearing (in tension) at the damaged half-wave even after members experience considerably large deformations (see Figure 1b and 2).

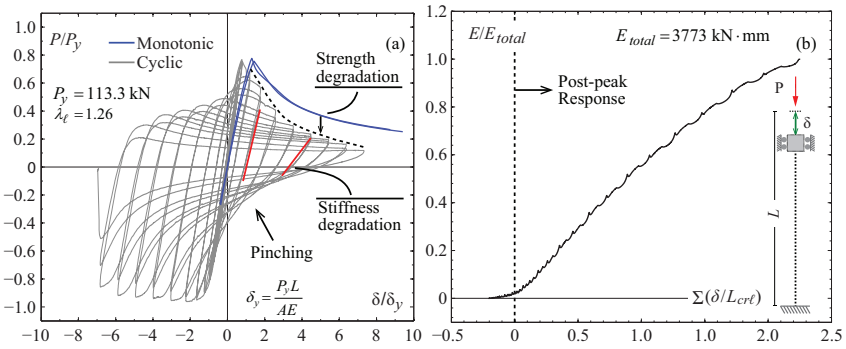

Figure 1. CFS axial members (a) typical *P*-δ response; and (b) cumulative energy dissipated.

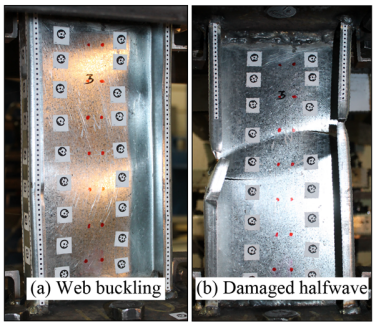

Figure 2. Local web buckling (a); and damaged half-wave with tearing (b).

Two approaches are introduced in this paper to model the axial cyclic load-deformation response of cold-formed steel members experiencing local buckling deformations: a *nonlinear spring* model with concentrated nonlinear *axial load-displacement* (*P*-δ), and a *nonlinear beam-column* with distributed nonlinear section *axial load-strain* (*P*-ε) behavior. Figure 3 illustrates both approaches for an axial member subjected to uniform axial loading. The underlying material model used in both approaches consists of a *backbone curve*, *unloading-reloading*

paths that account for pinching, and a *damage model* for strength and stiffness degradation (see Figure 3d). This formulation is based on the material model *Pinching4* as implemented in OpenSees (Lowes 2004, Mazzoni 2009).

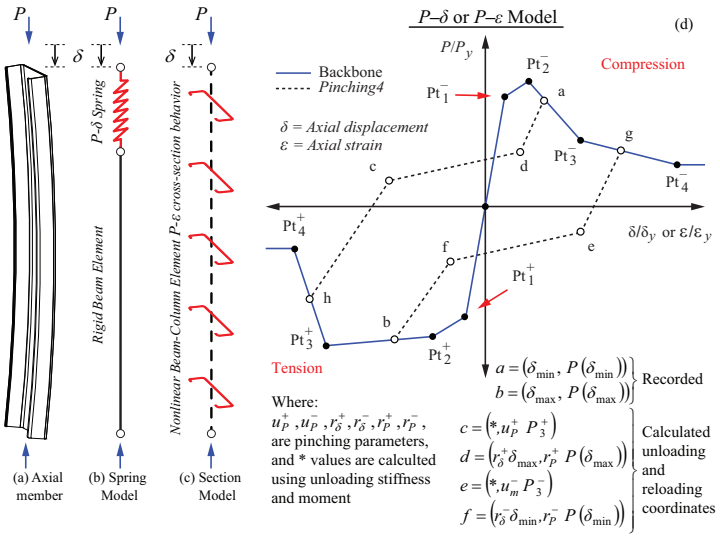

Figure 3. Axial hysteretic models for cold-formed steel axial members.

Spring models - concentrated nonlinearity

The spring modeling approach uses rigid beam elements connected to *nonlinear springs* where all the nonlinear behavior concentrates. Springs are located at preselected locations along the modeled member length and their number and distribution would depend on the loading conditions. Figure 3b illustrates this concept where the CFS member subjected to uniform axial loading in Figure 3a is modeled using a spring at the top end to capture the member axial cyclic response. For axial loads varying along the member length, additional springs should be located strategically such that the member response is accurately modeled. Backbone curves in tension and compression are derived from monotonic compression and tension tests. Strength and stiffness degradation parameters are obtained by direct calibration of *Pinching4* to match experimental cyclic responses and energy dissipation from the cyclic axial tests conducted by the authors (Padilla-Llano et al. 2014). The procedures to characterize and calibrate the nonlinear spring model are described elsewhere (Padilla-Llano et al. 2013) and the results for the CFS axial members experiencing local buckling are summarized here for convenience in Table 1 and Table 2.

Nonlinear beam-column model - distributed nonlinearity

A *nonlinear beam-column element* with distributed nonlinearity is defined using an axial load-strain P-ε formulation to model the response at the cross-section level (Figure 3c). This approach allows flexible modeling of CFS members subjected to different axial loading conditions (e.g. non-uniform axial load) using the same set of parameters that define the section behavior. The parameters to define the cross-section P-ε behavior are derived from the corresponding values defining the nonlinear spring model previously described. The strains coordinates in the backbone P-ε for axial CFS members subjected to uniform axial loading is obtained by dividing the axial displacements δ_i in Table 1 by the member length, thus, $\varepsilon_i = \delta_i / L$. Parameters to model strength degradation, stiffness degradation and pinching do not differ from those of the nonlinear spring model in Table 2.

Table 1. Backbone definition points for axial specimens (Padilla-Llano et al. 2013).

	Specimen[(a)]	P_y (kN)	k_e [(b)] (kN/mm)	δ_y [(b)] (mm)	δ_1/δ_y	δ_2/δ_y	δ_3/δ_y	δ_4/δ_y	P_1/P_y	P_2/P_y	P_3/P_y	P_4/P_y
								$\times 10^{-3}$				
	Compression											
1	600S162-33-LAM-1	71.5	143.5	0.499	526	816	2913	6000	385	427	259	188
2	600S162-33-LAM-2	71.6	143.6	0.499	608	1110	2234	6000	416	462	298	203
3	362S162-54-LAM-1	113.2	181.8	0.623	1017	1309	2877	6000	699	777	478	333
4	362S162-54-LAM-2	113.3	181.9	0.623	1108	1434	2791	6000	681	756	489	331
	Tension											
5	Tension Adjusted	113.8	182.8	0.623	1128	1488	6000	8000	1044	1134	1172	872

(a) SSMA profiles (SSMA 2011); AM=axial monotonic test; L=local buckling.
(b) $k_e = A_g E/L$ (E=203.4GPa); $\delta_y = P_y/k_e$.

Table 2. *Pinching4* model parameters (Padilla-Llano et al. 2013).

Specimen[(a)]	Damage Parameters						Pinching Parameters						Backbone Used [(c)]
	Strength		Stiffness				Compression			Tension			
	β_2	β_4	β_2	β_4	γ_E	E_M[(b)]	r_{D-}	r_{F-}	u_{F-}	r_{D+}	r_{F+}	u_{F+}	
600S162-33-LAC-1	0.71	0.55	0.68	0.33	8.68	294	0.48	0.92	0.50	0.80	0.30	-0.10	2, 5
600S162-33-LAC-2	0.78	0.73	0.73	0.33	8.47	293	0.48	0.92	0.50	0.80	0.30	-0.10	2, 5
362S162-54-LAC-1	0.55	0.49	0.66	0.43	6.63	579	0.48	0.92	0.50	0.53	0.62	-0.03	3, 5
362S162-54-LAC-2	0.56	0.46	0.62	0.32	6.49	581	0.49	0.92	0.50	0.53	0.62	-0.03	3, 5

(a) SSMA profiles (SSMA 2011); AC=axial cyclic test; L=local buckling.
(b) Energy in units of kN-mm; (c) Backbone curve from Table 1.

Both approaches are capable of modeling CFS member axial cyclic responses and both have their advantages. However, to apply these models to more general cases (i.e., different lengths and/or boundary conditions), it is necessary to explore how/where energy and damage accumulates in members experiencing local buckling for other conditions different than those used to derive the model parameters. If energy dissipation and damage accumulation occurs at one location as it was observed by Padilla-Llano et al. (2014), then the derived models can be used without further modifications. For this purpose, a small study, described

next, was carried out to investigate the length and boundary conditions effects on the energy dissipation and damage accumulation in cyclic axially loaded thin plates.

Energy dissipation in cold-formed steel thin plates

Energy dissipation in thin plates subjected to in plane cyclic axial loading was studied through finite element analysis in ABAQUS (ABAQUS 2013). The models are implemented using S9R5 thin shell elements for two sets of plates summarized in Table 3, including two width to thickness ratios (h/t), and different lengths (multiples of half-wavelength L_{cr}). The out of plane displacement (*2 direction, v=0*) around the edges is restrained such that edge nodes are free to move in the 1 and 3 (*u, w*) directions and free to rotate about direction 3. Two boundary condition cases for the loaded edges are considered to simulate pinned and fixed end conditions as shown in Figure 4a. Initial geometric imperfections are imposed based on the fundamental elastic buckling mode (see Figure 4a and 4c) with magnitudes d_0/t=0.17 and d_0/t=0.54. These magnitudes respectively correspond to occurrence probabilities $P(d<d_0)$=0.25 and $P(d<d_0)$=0.75 that the imperfection will be less than said value (Zeinoddini 2012). The elastic modulus of elasticity was assumed as E=203.4GPa and Poisson's ratio ν=0.3. Material nonlinearity plasticity was implemented using two *true* stress-strain (σ-ε) curves (Figure 4b) and isotropic hardening behavior. The plates are loaded from both ends with displacement control using the cyclic loading protocol for cold-formed steel members introduced by Padilla-Llano et al. (2014). The protocol is symmetric with steps of increasing amplitude and two cycles per step. Each step's amplitude is 40% larger than the previous (i.e., δ_i=1.4δ_{i-1}). The protocol is and is anchored at the fourth step to the elastic displacement $\delta_e=(0.673)^2P_{cr}L/AE$ where P_{cr} is the elastic plate buckling load (see Table 3).

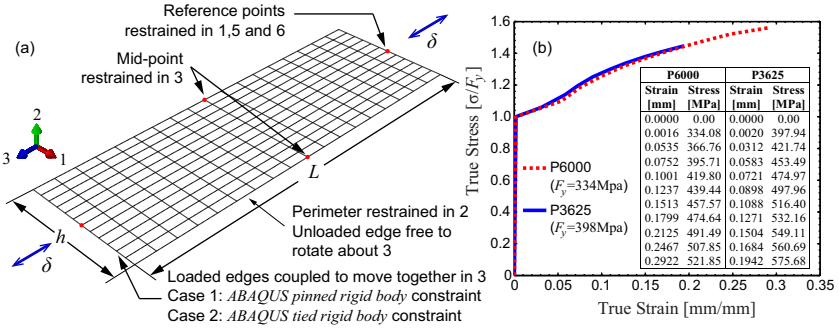

P6000		P3625	
Strain [mm]	Stress [MPa]	Strain [mm]	Stress [MPa]
0.0000	0.00	0.0000	0.00
0.0016	334.08	0.0020	397.94
0.0535	366.76	0.0312	421.74
0.0752	395.71	0.0583	453.49
0.1001	419.80	0.0721	474.97
0.1237	439.44	0.0898	497.96
0.1513	457.57	0.1088	516.40
0.1799	474.64	0.1271	532.16
0.2125	491.49	0.1504	549.11
0.2467	507.85	0.1684	560.69
0.2922	521.85	0.1942	575.68

Figure 4. Plate model (a) geometry and boundary conditions; and (b) assumed stress-strain curve.

Table 3. Simply supported thin plate analysis matrix summary.

Specimen[(a)]	t (mm)	h (mm)	L_{cr} (mm)	L	F_y (MPa)	P_{cr}[(a)] (kN)	Imperfection Magnitude [(b)]
P6000	0.879	147	147	1 to 10 times L_{cr},	334	3.24	d_0/t=0.17,
P3625	1.367	85	85	305 and 2740mm	398	20.90	and d_0/t=0.54

(a) Plate buckling load calculated for a square plate with $L=h=L_{cr}$.
(b) Occurrence probabilities $P(d<d_0)$=0.25 and $P(d<d_0)$=0.75 (Zeinoddini 2012)

The axial cyclic responses obtained show elastic behavior for all cycles before reaching the peak compression load. At the peak compression load, energy dissipation starts as plastic strains concentrate at one or more locations leading to full cross-section and plate collapse (i.e., no load carrying capacity either in compression or tension). Damage accumulated in this zones that are approximately one half-wave (L_{cr}) long for all the plates analyzed irrespective of the plate length and generally happened at the mid-length (see, Figure 5b). This behavior is consistent with the results reported by Padilla-Llano et al. (2014) where energy dissipation and damage accumulation happened in only one location. Such behavior can be modeled using the approaches described in the previous section where nonlinear behavior is either lumped to a spring or averaged along the length of a member under uniform axial load. Only in four plates, corresponding to the longer plates with ratio h/t=62.12, fixed ends (case 2 in Figure 4), and symmetric imposed imperfection patterns, the damaged zones happened closer to the loaded ends as shown in Figure 5d. Energy dissipation occurs through plastic deformation at the damaged zones.

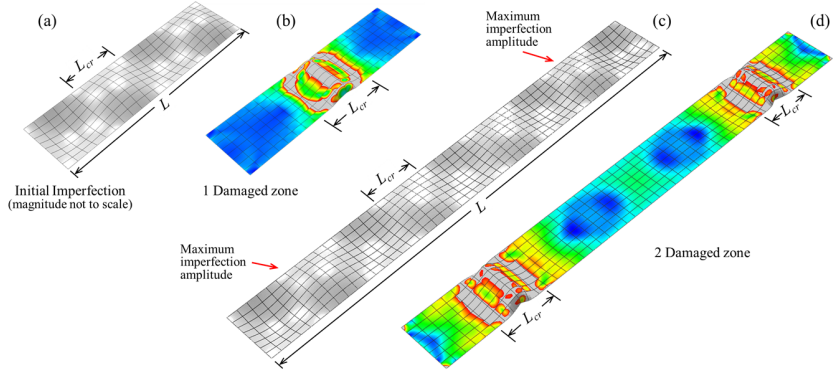

Figure 5. Initial imperfection shape and damaged zone relationship in cyclic axially loaded plates.

Cumulative energy dissipation is compared in Figure 6 for all lengths and for the two imperfection magnitudes considered. The energy dissipated was normalized to $P_y\delta_{cr}$ ($P_y=AF_y$, $\delta_{cr}=P_yL_{cr}/AE$, $A=th$) and plotted as a function of the cumulative post-peak applied displacement divided the half-wave length $\Sigma(\delta/L_{cr})$. It can be seen that all the curves are grouped and therefore energy dissipation is independent of the plate length and is confined to a damaged zone that extends approximately a half-wave length L_{cr}. In the four long plates (L=849mm and 2743mm) that exhibited two damaged zones close to the loaded edges as shown in Figure 5d, the amount of energy dissipation was about twice as much the plates that exhibited only one damaged zone (see Figure 6b). Thus, the amount of energy dissipated is proportional to the number of damaged zones developed in the plate (i.e., zones with concentration of plastic strains).

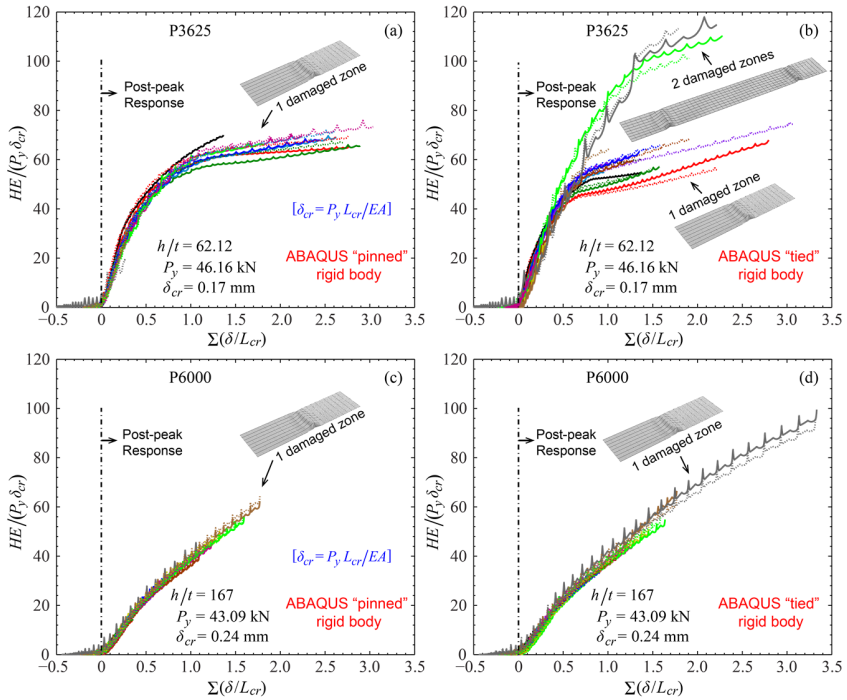

Figure 6. Cumulative hysteretic energy (*HE*) dissipated in cyclic axially loaded thin plates of various lengths: (a) width h=85mm pinned ends; (b) width h=85mm tied ends; (c) width h=147mm pinned ends; (d) width h=147mm tied ends (see Table 3).

The presence of two damaged zones is related to the initial geometric imperfection field imposed to the plates. The imperfection field imposed to the long plates (i.e., fundamental buckling mode) present maximum amplitudes towards the loaded edges. The magnitude of the imperfection (i.e., d_0/t=0.17 and d_0/t=0.54) had no effect on the amount of energy dissipated or location of the damage zone. The results from this plate study are consistent with the observed behavior and energy dissipation of cyclic axially loaded cold-formed steel members that experienced local buckling described by Padilla-Llano et al. (2014).

Simulating CFS members axial cyclic response

The two models, *nonlinear springs* and the *nonlinear beam-column* element illustrated in Figure 3 are used to simulate the response of CFS axial members experiencing local buckling tested by Padilla-Llano et al. (2014). The spring model is implemented using rigid beam elements connected to *zeroLength* elements in OpenSees that is located at the loaded end as shown in Figure 7b. For these models, one spring will suffice and values from Table 1 and 2 are used directly without further adjustment that would be required for example if additional springs were to be placed along the member length. The nonlinear beam-column model is implemented in OpenSees using *dispBeamColumn* elements connected between the two end nodes (see Figure 7b). The Gauss-Lobatto quadrature rule with seventh interpolation points, two at the element ends, is used for numerical integration within each element. Axial load-strain section behavior is implemented using values from Table 1 and 2 with $\varepsilon_i = \delta_i/L$.

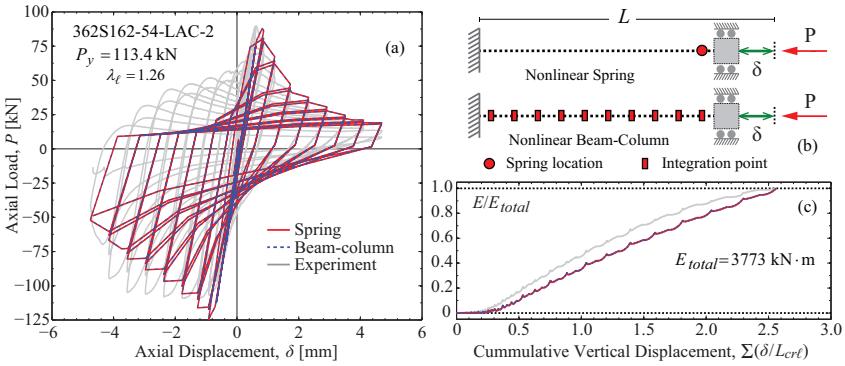

Figure 7. Simulated and experimental response (a); spring and beam-column models (b); energy dissipated (c).

Comparison between the two modeling approaches shows that both produce similar results as far as modeling the experimental load-deformation cyclic response P-δ as illustrated in Figure 7a. The root mean-squared deviation between the predicted load responses to the tests is between 8% and 14%. Both approaches show very similar energy dissipation cycle by cycle (Figure 7c) and the total energy dissipated is almost identical. The hysteretic energy dissipated by the simulated responses develop slower than the experiments as evidenced by Figure 7c with E_{model}/E_{total}=0.94 (cov=0.09) at fracture (Padilla-Llano et al. 2013). Spring models with rigid bars have the disadvantage of displacement incompatibility depending on the spring arrangement that also requires adjustment of spring definition parameters. Using a beam-column element with distributed nonlinearity P-ε is a more flexible approach that permits modeling for different loading conditions using the same set of parameters defining the section behavior derived from Table 1 and 2.

Conclusions

This paper presented two approaches to model the cyclic axial response of CFS member showing that both, the nonlinear spring and the nonlinear-beam column models can capture the axial member cyclic response efficiently. However, spring models can present disadvantages such as displacement and/or rotation compatibility and difficulty adapting the model to different loading configurations such as non-uniform axial loading, or axial loading combined with bending. In this regard, the beam-column element with distributed nonlinearity P-ε is a more flexible approach that permits modeling for different loading conditions using the same set of parameters defining the section behavior. The authors continue to explore this last approach and others based on distributed nonlinear behavior for modeling cyclic behavior of thin-walled cold-formed steel members and its application to light steel framed building systems.

Acknowledgements

The authors are grateful to the American Iron and Steel Institute (AISI) for funding this research and to the AISI Project Monitoring Task Group especially Bonnie Manley, Ben Schafer, Jay Larson, Colin Rogers, and Steve Tipping.

References

ABAQUS (2013). ABAQUS Documentation v6.13, Dassault Systèmes Simulia Corp., Providence, RI, USA.

AISI S213-07, (2007a), North American Standard for Cold-Formed Steel Framing: Lateral Design, American Iron and Steel Institute, Washington, D.C. ANSI/AISI-S213-07.

AISI-S100-07 (2007b) North American Specification for the Design of Cold-Formed Steel Structural Members. American Iron and Steel Institute, Washington, D.C. ANSI/AISI-S100-07.

FEMA, (2009), FEMA P695-Quantification of Building Seismic Performance Factors, Federal Emergency Management Agency (FEMA), Document No. FEMA 965, Washington, D.C.

Lowes, L., Mitra, N., Altoontash, A., (2004). A Beam-Column Joint Model for Simulating the Earthquake Response of Reinforced Concrete Frames, PEER Report 2003/10, Pacific Earthquake Engineering Research Center.

Mazzoni, S., McKenna, F., Scott, M.H., Fenves, G.L., (2009). Open System for Earthquake Engineering Simulation User Command-Language Manual, OpenSees Version 2.0, Berkeley, California.

Padilla-Llano, D., Eatherton, M., Moen, C., (2013a), "Axial Hysteretic Modeling of Cold-Formed Steel Members for Computationally Efficient Seismic Simulation." Structures Congress 2013, American Society of Civil Engineers, 948–959.

Padilla-Llano, D., Moen, C., Eatherton, M., (2013b), Energy Dissipation of Thin-Walled Cold-Formed Steel Members. Virginia Polytechnic Institute and State University Research Report No. CE/VPI-ST-13/06, Blacksburg, VA.

Padilla-Llano, D., Moen, C., Eatherton, M., (2014), Cyclic axial response and energy dissipation of cold-formed steel framing members, Thin-Walled Structures, vol. 78, pp. 95–107.

SSMA (2011), Steel Stud Manufacturers Association, Product Technical Information, ICBO ER-4943P, <http://www.ssma.com >, (December 15, 2011).

Zeinoddini V., Schafer B., (2012), Simulation of geometric imperfections in cold-formed steel members using spectral representation approach, Thin-Walled Structures; vol. 60, pp. 105–17.